ACS APPLIED MATERIALS & INTERFACES

Research Article

www.acsami.org

Boron and Nitrogen Codoped Carbon Layers of $LiFePO_4$ Improve the High-Rate Electrochemical Performance for Lithium Ion Batteries

Jinli Zhang,[†,‡] Ning Nie,[†] Yuanyuan Liu,[†] Jiao Wang,[†] Feng Yu,[‡] Junjie Gu,[§] and Wei Li*[,†]

[†]School of Chemical Engineering, Tianjin University, Tianjin 300072, China

[‡]Key Laboratory for Green Processing of Chemical Engineering of Xinjiang Bingtuan, School of Chemistry and Chemical Engineering, Shihezi University, Shihezi 832003, China

[§]Department of Mechanical and Aerospace Engineering, Carleton University, Ottawa, Ontario K1S 5B6, Canada

Supporting Information

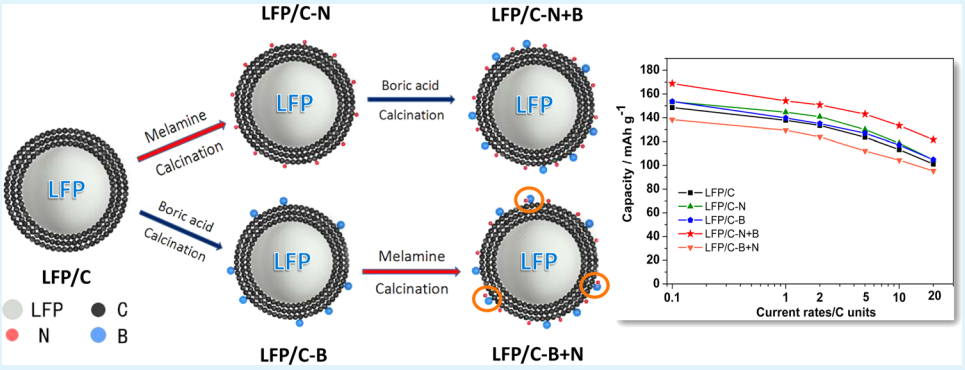

ABSTRACT: An evolutionary composite of $LiFePO_4$ with nitrogen and boron codoped carbon layers was prepared by processing hydrothermal-synthesized $LiFePO_4$. This novel codoping method is successfully applied to $LiFePO_4$ for commercial use, and it achieved excellent electrochemical performance. The electrochemical performance can be improved through single nitrogen doping ($LiFePO_4$/C−N) or boron doping ($LiFePO_4$/C−B). When modifying the $LiFePO_4$/C−B with nitrogen (to synthesis $LiFePO_4$/C−B+N) the undesired nonconducting N−B configurations (190.1 and 397.9 eV) are generated. This decreases the electronic conductivity from 2.56×10^{-2} to 1.30×10^{-2} S cm^{-1} resulting in weak electrochemical performance. Nevertheless, using the opposite order to decorate $LiFePO_4$/C−N with boron (to obtain $LiFePO_4$/C−N+B) not only eliminates the nonconducting N−B impurity, but also promotes the conductive C−N (398.3, 400.3, and 401.1 eV) and C−B (189.5 eV) configurations—this markedly improves the electronic conductivity to 1.36×10^{-1} S cm^{-1}. Meanwhile the positive doping strategy leads to synergistic electrochemical activity distinctly compared with single N- or B-doped materials (even much better than their sum capacity at 20 C). Moreover, due to the electron and hole-type carriers donated by nitrogen and boron atoms, the N+B codoped carbon coating tremendously enhances the electrochemical property: at the rate of 20 C, the codoped sample can elevate the discharge capacity of LFP/C from 101.1 mAh g^{-1} to 121.6 mAh g^{-1}, and the codoped product based on commercial $LiFePO_4$/C shows a discharge capacity of 78.4 mAh g^{-1} rather than 48.1 mAh g^{-1}. Nevertheless, the B+N codoped sample decreases the discharge capacity of LFP/C from 101.1 mAh g^{-1} to 95.4 mAh g^{-1}, while the commercial LFP/C changes from 48.1 mAh g^{-1} to 40.6 mAh g^{-1}.

KEYWORDS: *lithium iron phosphate, carbon coating, nitrogen doping, boron doping, lithium ion batteries, electrochemical energy storage*

1. INTRODUCTION

Conductive surface modifications toward carbon coating of olivine-structured lithium iron phosphate ($LiFePO_4$) have attracted significant attention due to its high efficiency and environmental benevolence in the development of lithium ion battery cathode materials.[1−5] As an advanced cathode material for commercial use, $LiFePO_4$ has its drawbacks such as small electronic conductivity and a weak Li^+ diffusion coefficient, which restricts it from the large-scale applications in high performance. Besides upgrading surface carbon coating, plenty of trials have been attempted to improve the electrochemical properties of $LiFePO_4$-based cathode material including narrowing particle size or changing its morphology,[6−8] alien ion doping or substitution,[9−11] and adding conductive agents onto the surface.[12−14] However, methods to improve the conductive surface carbon coatings are still promising for enhancing the electrochemical performance, along with controlling the carbon content at an appropriate level (excessive

Received: June 17, 2015
Accepted: August 25, 2015
Published: August 25, 2015

DOI: 10.1021/acsami.5b05398
ACS Appl. Mater. Interfaces 2015, 7, 20134−20143

carbon may lead to a lower Li^+ diffusion rate and less $LiFePO_4$-active component). Recently, a graphene wrapped cathode material "$LiFePO_4$/C/graphene" was successfully synthesized to meet the needs of high-efficiency and low-cost improvement through the carbon coating modification.[15] Therefore, it is intriguing to put forward novel methods to modify conductive carbon coatings, so as to enhance further the rate performance of $LiFePO_4$.

Comparing with ordinary carbon coating, the heteroatom-incorporated carbon materials, in particular, nitrogen-doped and boron-doped, exhibit a better electron transfer rate.[16] It has been proposed that the nitrogen-doped carbon layers can efficiently facilitate electronic conductivity of the material since nitrogen atoms act as an electron donor and provide electron carriers and decrease the band gap.[17−19] N-doped carbon has been successfully used to improve electrochemical performance involving $LiFePO_4$ and nanotubes.[20−22] On the other hand, boron-doping can also elevate the carbon conductivity by increasing the quantity of hole-type charge carriers and transforming the electroneutrality of carbon-containing materials.[23]

Inspired by the electron acceptor (boron) and donor (nitrogen) being one electron away from carbon, $LiFePO_4$ with N and B codoped carbon layers were studied. We are eager to investigate whether or not N and B codoped carbon coatings can improve the electrochemical property of $LiFePO_4$/C. To the best of our knowledge, so far there is no literature concerning N and B codoped carbon layers on the surface of $LiFePO_4$. Herein, we successfully incorporated nitrogen and boron into the carbon layers with desirable molar ratio and obtained totally opposite electrochemical performance by reversing the B−N addition sequence. The effects of N-doping, B-doping, N+B codoping, as well as counterpart B+N codoping were studied, in combination with characterizations of the electrochemical performance, phase purity, and morphology. We also applied the codoping strategy to the commercial powders $LiFePO_4$/C to confirm further the improvement of electrochemical performance via N+B codoping.

2. EXPERIMENTAL SECTION

2.1. Sample Preparation. Lithium iron phosphate with carbon coating ($LiFePO_4$/C) was prepared by a simple hydrothermal method with the Li:Fe:P molar ratio of 3:1:1, using LiOH, $FeSO_4$, and H_3PO_4 as original materials and glucose as the carbon source, and the concentration of Fe^{2+} was 0.5 mol L^{-1}. Using a high shear mixer,[24] the solution of glucose and H_3PO_4 was dropped into LiOH, followed by $FeSO_4$ under vigorous stirring at the speed of 1.3×10^4 rpm and nitrogen atmosphere. The obtained suspension was input into an autoclave and heated to 180 °C for 3 h under stirring. Subsequently, the filtered precipitate was washed and dried at 120 °C, followed by calcination at 700 °C for 6 h under nitrogen to produce $LiFePO_4$/C with the carbon content of 2.0% measured by the TG analysis results, which was denoted as LFP/C in this context.

Single-element doping materials, involving $LiFePO_4$/C−N and $LiFePO_4$/C−B, were prepared via the ball-milling procedure followed by calcination at 600 °C for 4 h (with a heating rate of 5 °C min^{-1}) under nitrogen flow. For instance, the N-doped $LiFePO_4$/C−N125 sample was prepared by ball-milling 8 g as-prepared LFP/C with 0.352 g melamine (99.5%, Guangfu) so as to generate the N:C molar ratio of 125%, which was denoted as LFP/C−N, while the B-doped $LiFePO_4$/C−B25 sample was prepared by ball-milling 8 g as-prepared LFP/C with 0.21 g boric acid (99.99%, HEOWNS) so as to generate the B:C molar ratio of 25%, which was denoted as LFP/C−B. We also prepared N-doped $LiFePO_4$/C−N samples with the N:C molar ratio of 25% and 150%, and B-doped $LiFePO_4$/C−B samples with the B:C molar ratio of 6%, 12.5%, 25%, and 125%; however, the electrochemical performance results of these samples are respectively lower than that of $LiFePO_4$/C−N125 and $LiFePO_4$/C−B25, as shown by Figure S1 and Figure S2 in the Supporting Information.

The N and B codoping materials were produced via a secondary ball-milling from the single doping LFP/C−N or LFP/C−B, adopting the optimal molar ratio of N:C and B:C. The $LiFePO_4$/C−N125+B25 sample was prepared by ball-milling 0.105 g B and 4 g N-doped LFP/C−N followed by calcination at 600 °C for 4 h, so as to generate the B:C molar ratio of 25%, which was denoted as the codoping sample LFP/C−N+B, while the counterpart sample $LiFePO_4$/C−B25+N125 was prepared by ball-milling 0.176 g N and 4 g B-doped LFP/C−B, followed by washing the residue B_2O_3 via hot water (70 °C) and consequently similar calcination, to generate the N:C molar ratio of 125%, which was denoted as the codoping sample LFP/C−B+N.

As a control, the commercial powder of $LiFePO_4$ with a carbon-coating layer on its surface (the carbon content in $LiFePO_4$ was 2.0%), manufactured through the solid-state method, was purchased from Li Zhi Yuan lithium China. Such commercial $LiFePO_4$/C was denoted as c-LFP/C, and treated by the corresponding doping procedure mentioned above to produce respectively the single-doping samples of c-LFP/C−N, c-LFP/C−B, and the codoping samples of c-LFP/C−N+B, c-LFP/C−B+N.

2.2. Structural and Morphological Characterizations. The as-prepared samples were detected using X-ray diffraction (XRD, Panalytical) utilizing Cu Kα radiation (λ = 0.154 nm) at 40 kV and 40 mA, collecting data from 15° to 65° (2θ deg) in steps of 4° min^{-1}. HR-TEM images were performed by a high resolution transmission electron microscope (JEM100CXII) at 100 kV. SEM mapping was characterized using FEI Quanta200 SEM. TG analysis was detected on a Netzsch-STA 449C from 25 to 700 °C at a heating rate of 10 °C min^{-1} in the air. XPS spectra were performed by a PHI5000 Versa Probe spectrometer with a monochromatized Al Kα X-ray source and an analyzer pass energy of 187.85 eV for scanning. Inductively coupled plasma emission spectrometer (ICP, Varian 725-ES) was used to measure the boron content, with the samples dissolved using a Microwave extraction system (MARS 240/50). The nitrogen content was confirmed by the Qxygen-Nitrogen Analyzer (ON3000).

2.3. Electrochemical Measurements. Electrochemical measurements were performed at room temperature using CR2032 coin-type cells with the lithium as the counter electrode. The cathodes were prepared using the mixture of as-prepared single- or codoping $LiFePO_4$/C materials, acetylene black, and polyvinylidene fluoride (PVDF) with a weight ratio of 8:1:1. The slurry was spread onto the aluminum foil, followed by drying at 120 °C for 12 h under vacuum.

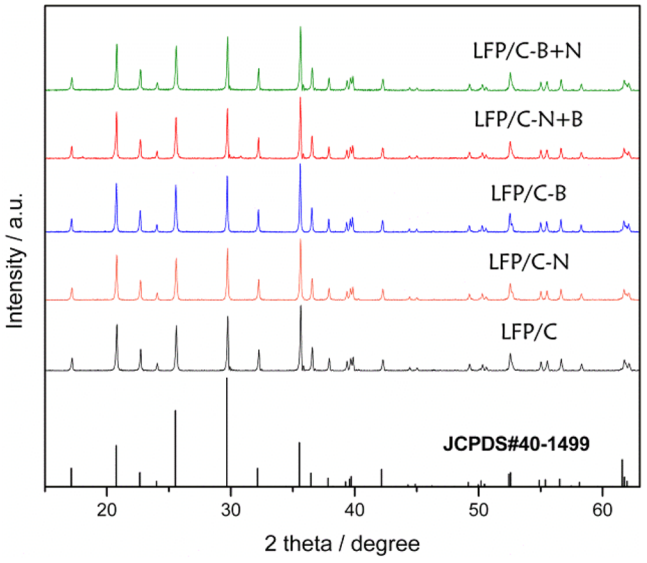

Figure 1. XRD patterns of LFP/C, LFP/C−N, LFP/C−B, LFP/C−N+B, LFP/C−B+N.

DOI: 10.1021/acsami.5b05398
ACS Appl. Mater. Interfaces 2015, 7, 20134−20143

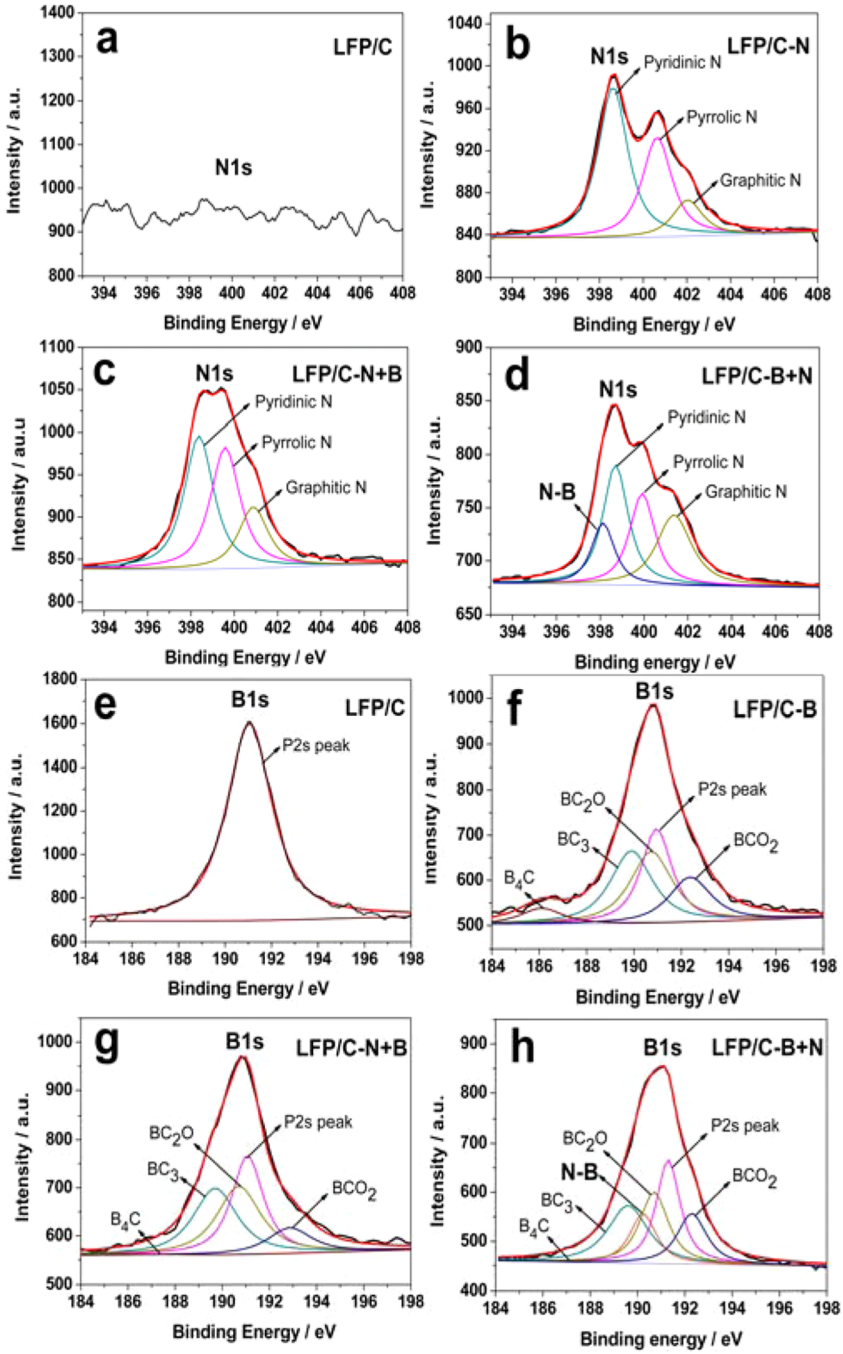

Figure 2. XPS spectra of samples with N dopant: (a) LFP/C, (b) LFP/C−N, (c) LFP/C−N+B, (d) LFP/C−B+N; and B dopant: (e) LFP/C, (f) LFP/C−B, (g) LFP/C−N+B, (h) LFP/C−B+N.

Table 1. Distribution of Bond Types and Peak Area Ratio Based on N 1s

	binding energy/eV				peak area ratio/%			
Sample	Pyridinic N	Pyrrolic N	Graphitic N	N−B	Pyridinic N	Pyrrolic N	Graphitic N	N−B
LFP/C−N	398.6	400.6	401.3	-	52.6	34.8	12.6	-
LFP/C−N+B	398.4	400.6	401.0	-	42.1	38.4	19.4	-
LFP/C−B+N	398.6	400.2	401.3	398.1	44.5	23.0	26.0	6.5

A mixed solvent of ethylene carbonate (EC)−dimethyl carbonate (DMC) containing 1 M $LiPF_6$ was served as the electrolyte. The coin-type cell was assembled in an argon-filled glovebox, where the contents of H_2O and O_2 were both less than 0.1 ppm with Celgard 2400 as the separator. The charging−discharging experiments were performed on the LAND-CT2011A test system (Wuhan, China) with the voltages ranging from 2.0 to 4.2 V versus Li/Li^+. The electrochemical impedance spectroscopic analysis (EIS) was performed on CHI660E (CH Instruments, China) by using a 0.005 V amplitude signal, with the frequency ranging from 0.1 Hz to 100 kHz. The conductivities of samples were tested on RTS-9 by a four-point probe technique.

DOI: 10.1021/acsami.5b05398
ACS Appl. Mater. Interfaces 2015, 7, 20134−20143

Table 2. Distribution of Bond Types and Peak Area Ratio Based on B 1s

	Binding energy/eV						Peak area ratio/%					
Sample	P 2s	B_4C	BC_3	B−N	BC_2O	BCO_2	P 2s	B_4C	BC_3	B−N	BC_2O	BCO_2
LFP/C−B	191.0	187.2	189.7	-	190.7	192.5	25.2	5.8	26.5	-	26.1	16.4
LFP/C−N+B	191.1	187.5	189.7	-	190.7	192.8	30.7	0.3	28.7	-	29.4	11
LFP/C−B+N	191.1	187.5	189.5	190.2	190.7	192.5	25.5	0.8	20.2	16.7	21.3	15.4

3. RESULTS AND DISCUSSION

Figure 1 shows XRD patterns of single-doping and codoping $LiFePO_4$ materials. The five kinds of as-prepared materials show intense and spiculate peaks that can be indexed to the olivine-structured $LiFePO_4$ phase of the *Pnma* space group (JCPDS card NO.40−1499) and no extra phase is detected, confirming the high phase purity and lack of structural destruction generated by the N-/B-doping process.

The nature of doping and codoping samples is identified based on the deconvoluted XPS spectra of N 1s (Figure 2a−d) and B 1s (Figure 2e−h). For N-containing samples (LFP/C−N, LFP/C−N+B, LFP/C−B+N), it is obvious that all N atoms are incorporated into the neighboring carbon layers to form the structure involving the Pyridinic N (398.3 eV), the Pyrrolic N (400.3 eV), and the Graphitic N (401.1 eV).[25] It is noteworthy to mention the new peak near 397.9 eV in the sample LFP/C−B+N, which is due to the N−B configuration[26] (Figure 2d). Table 1 lists the relative content of these four types of N species in the samples of LFP/C−N, LFP/C−N+B, and LFP/C−B+N. It is clear that the N−B configuration is only generated in LFP/C−B+N, with the doping order of B followed by N. Such an N−B configuration is proven to work as an impurity resulting in poor conductivity in the following section.

Figure 2e−h displays the deconvoluted XPS spectra of B 1s for B-containing samples LFP/C−B, LFP/C−N+B, and LFP/C−B+N. For the undoped LFP/C, there is a peak at 191.05 eV due to the inherent P 2s from $LiFePO_4$.[27] For B-doped samples of LFP/C−B and LFP/C−N+B, there are peaks located, respectively, at 187.5 eV due to B_4C type bond,[28] 189.5 eV due to BC_3,[28−30] and 190.8 and 192.7 eV attributed to the bond of BC_2O and BCO_2,[31] while for LFP/C−B+N, there is a peak at 190.1 eV attributed to the N−B bond,[32] in accord with the deconvolution of N 1s XPS spectra.

Table 2 lists the B-containing species in samples determined through the deconvolution of B 1s XPS spectra. It is shown that the relative content of the B_4C bond is the lowest in each sample, which is associated with carbon defects,[33] and its effect on electrochemical performance is ignored. The content of BC_3 increases in the order of LFP/C−B+N (20.2%) < LFP/C−B (26.5%) < LFP/C−N+B (28.7%), while the sums of BC_2O and BCO_2 in these three samples are close to each other (~40%). In particular, only the sample LFP/C−B+N contains the N−B bond. The individual content of nitrogen and boron in the codoped product LFP/C−B+N is 0.11 and 0.0345 wt %, respectively, determined by the elemental analysis. According to the relative atomic mass of nitrogen (14) and boron (11), the molar ratio N/B is calculated to be 2.5:1. Based on the content of N−B configuration derived from B 1s spectra (16.7%, Table 2), the corresponding content is calculated as 16.7%/2.5 = 6.7%, which is approximate to the N−B content determined according to the N 1s XPS spectra (6.5%, Table 1). Hence, these results illustrate that the doping sequence of N+B is beneficial to form BC_3 in the carbon coatings, which plays an important role in altering the valence band structure of carbon-based materials and increasing the density of states near the Fermi level,[34] and consequently improves the electronic conductivity. In contrast, the reverse doping sequence of B+N results in a lower content of conductive BC_3, but the emergence of the N−B configuration.

Table 3. Powder Electronic Conductivities of LFP/C, LFP/C−N, LFP/C−B, LFP/C−N+B, and LFP/C−B+N

material	conductivity/$\times 10^{-2}$ S cm^{-1}
LFP/C	2.56
LFP/C−N	7.57
LFP/C−B	6.33
LFP/C−N+B	13.6
LFP/C−B+N	1.30

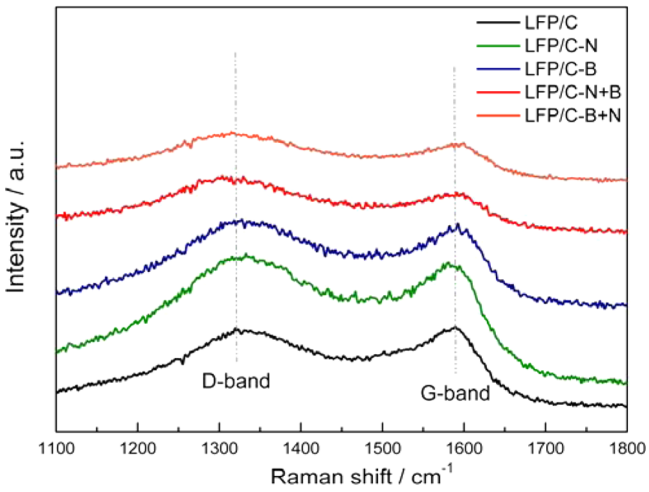

Figure 3. Raman spectrum of LFP/C, LFP/C−N, LFP/C−B, LFP/C−N+B, and LFP/C−B+N.

Table 4. I_D/I_G Value of Five Samples

sample	I_D/I_G
LFP/C	0.91
LFP/C−N	1.16
LFP/C−B	1.12
LFP/C−N+B	1.30
LFP/C−B+N	1.29

To disclose the influence of the N−B configuration on conductivity, powder electronic conductivities of these samples were examined using the 4-point probe method. Table 3 lists the electronic conductivities of five kinds of samples. It is clear that LFP/C−N+B has the highest conductivity (13.6×10^{-2} S cm^{-1}), much higher than that of LFP/C−B+N (1.30×10^{-2} S cm^{-1}), indicating that the existence of N−B configuration can reduce greatly the electronic conductivity, even lower than that of the undoped LFP/C (2.56×10^{-2} S cm^{-1}). Previously, through density functional theory calculations[35,36] it

DOI: 10.1021/acsami.5b05398
ACS Appl. Mater. Interfaces 2015, 7, 20134−20143

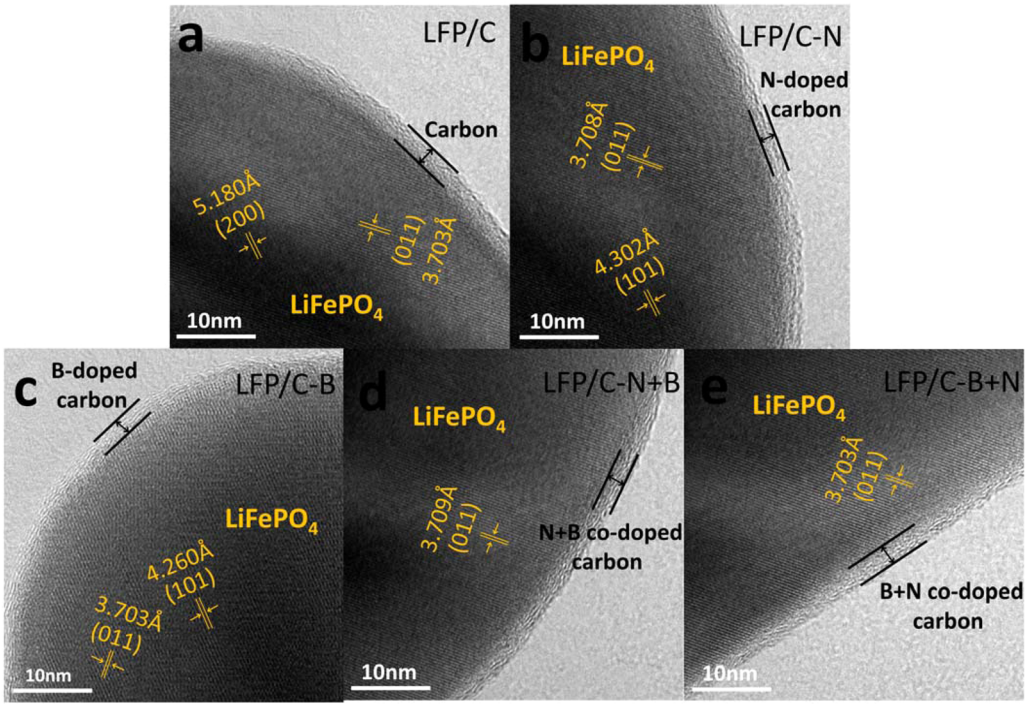

Figure 4. HRTEM images of LFP/C (a), LFP/C−N (b), LFP/C−B (c), LFP/C−N+B (d), and LFP/C−B+N (e).

was reported that the electric conductivity of $LiFePO_4$ coated with graphene-like B−C−N could have high electrochemical performance. However, herein the results indicate for the first time that the doping sequence of N−B played a crucial role in enhancing the conductive BC_3 configuration but inhibiting the nonconductive N−B configuration, which can result in the substantial increase of electrochemical performance of $LiFePO_4$.

The single doped and codoped carbon layers on the surface of $LiFePO_4$ were detected using Raman spectra (Figure 3). The two prominent peaks are related to the D-band (1325 cm^{-1}) and G-band (1592 cm^{-1}), respectively. The intensity of the D-band is related to the irregular levels of carbon materials, while the G-band is associated with the vibration mode of the sp^2-bonded carbon atoms. It is known that the intensity ratio of the D-band and the G-band (I_D/I_G) can reflect the extent of defects in the carbon materials and the graphitization of the surface carbon.[37,38] As listed in Table 4, the four doping samples have higher I_D/I_G values than undoped LFP/C, suggesting that heteroatom doping results in more defects in the surface carbon coating of $LiFePO_4$/C. In previous reports using boron or nitrogen doping,[23,39,40] the topological defects introduced through doping may reduce the degree of graphitization and facilitate more electrochemical active sites for lithium ion passage. This eventually improves the electrochemical properties of the material. The $LiFePO_4$/C−N+B sample has the highest I_D/I_G ratio of 1.30, which exhibits excellent electrochemical performance. Moreover, the B+N codoped sample with a relatively higher I_D/I_G ratio has not yet revealed the equivalent electrochemical properties, owing to the formation of nonconductive N−B impurities.

The HR-TEM images of the five composites, as shown in Figure 4, indicate that the original LFP/C and the doped samples are surrounded with a fairly uniform 2 nm carbon coating (Figure 4a−e). The interplanar spacing values are 5.180 Å, 3.703 Å (including 3.708 Å, 3.709 Å) and 4.302 Å (4.260 Å), corresponding to the lattice planes (200), (011), and (101) of the $LiFePO_4$ phase, which demonstrates good crystallinity for higher Li^+ diffusion rates. To confirm the carbon content in each sample, the TG analysis is used and the calculated weight ratio of carbon in sample LFP/C, LFP/C−N, LFP/C−B, LFP/C−N+B, and LFP/C−B+N is 2.0, 2.1, 1.9, 2.1, and 2.0 wt %, respectively. It is indicated that the single-doping or codoping process has little influence on the carbon content coated on the surface of $LiFePO_4$.

SEM mapping of five samples was performed to deeply understand the distribution of B and N in the doped samples. According to SEM mapping images, as shown in Figures S3−S8 in the Supporting Information, it is obvious that Fe, P, and O were distributed uniformly along with the morphology of the particle. As for the C distribution, the signals are weak owing to the disturbance of abundant C-containing compound in the electroconductive paste used to prepare each SEM sample. In combination with the carbon layers shown in Figure 4, it is reasonable to conclude that the C also has a uniform distribution in each particle. For the N-doped materials, the distribution of N element is uniform although its content is low and the signal is weaker than that of Fe, P, and O elements, while for the B-doped materials, it is hard to obtain effective signal because the content of B is lower than the EDS detection limit.

Figure 5a−e shows the electrochemical performance of single-doped and codoped $LiFePO_4$ samples based on LFP/C. According to the initial galvanostatic charge−discharge voltage profiles at a 0.1 C rate, all five samples have a flat voltage plateau at approximately 3.4 V (versus Li^+/Li), which implies the Fe^{2+}/Fe^{3+} redox reaction. The initial discharge capacity of LFP/C is around 148.6 mAh g^{-1}, while N-doped, B-doped, and N+B codoped samples exhibit higher discharge capacities of 151.2, 153.7, and 166.8 mAh g^{-1}, respectively. However, the B+N codoped sample has a reverse adding sequence with a low discharge capacity of 138.4 mAh g^{-1}. Higher plateau capacity and higher efficiencies may have positive effects on providing longer sustainable running time in electronic equipment. At the

DOI: 10.1021/acsami.5b05398
ACS Appl. Mater. Interfaces 2015, 7, 20134−20143

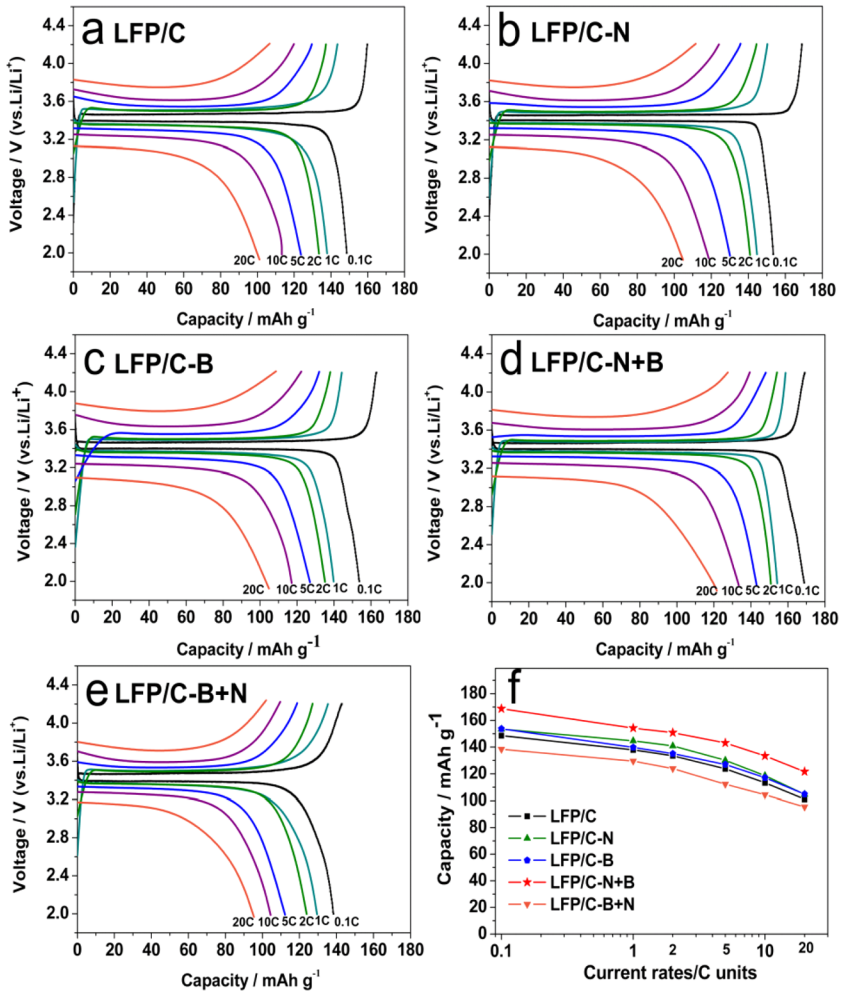

Figure 5. Electrochemical performance of doping (codoping) samples at different current densities in the potential window 2.0−4.2 V: (a−e) charge−discharge tests for LFP/C, LFP/C−N, LFP/C−B, LFP/C−N+B, and LFP/C−B+N at various C rates between 0.1 and 20 C, respectively; (f) Specific capacity of five samples at various C rates.

rate of 0.1 C in the initial cycle (Figure S9a), the Coulombic efficiency values are 92.0%, 91.0%, 94.3%, 98.6%, and 95.0% for LFP/C, LFP/C−N, LFP/C−B, LFP/C−N+B, and LFP/C−B+N, respectively. The LFP/C−N+B sample owns the optimal electrochemical performance, indicating that nitrogen and boron codoping can improve not only the platform capacity, but the Coulombic efficiency of carbon coating $LiFePO_4$ materials as well. With the increase of current rates, the capacities of the five samples decay, which is due to polarization in the electrode (Figure 5f). At 1 C, the LFP/C−N+B and LFP/C can achieve a discharge capacity of 154.2 mAh g^{-1} and 137.9 mAh g^{-1}, which are 92.4% is 92.8% of the maximum capacity at 0.1 C, respectively. At 2 and 5 C, the N+B codoped sample delivers 90.4% and 85.8% rather than 89.8% and 83.2%. At the rate as high as 20 C, the reversible capacity of 121.6 and 101.1 mAh g^{-1} can be achieved. This indicates that the N+B codoped sample has better capacity retention than LFP/C. The polarization becomes obvious with increasing current rates, but in each rate the LFP/C−N+B has better capacity retention. Moreover, at the high rate of 20 C, compared to the original material, the nitrogen and boron codoped sample has a much higher enhancement in capacity than the sum of nitrogen and boron. This surprising result proves that there are extra synergistic effects between nitrogen and boron in capacity improvement rather than simple superposition. This phenomenon can also be found in the codoped commercial c-LFP/C shown below.

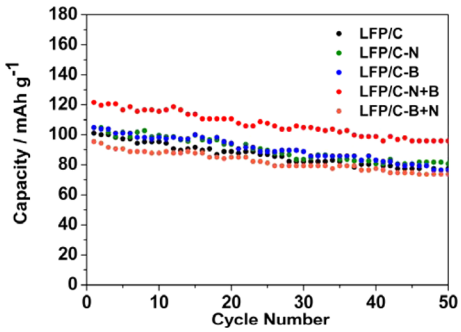

Figure 6. Cycle performance at 20C.

Further, the electrochemical performance at higher current rates of 1, 2, 5, 10, and 20 C are shown in Figure S9b. In comparison with the undoped LFP/C sample, the single N- or B-doped and the N+B-codoped samples show obvious enhancement in capacity at every current density. The LFP/C−N+B sample, especially, shows a supreme discharge capacity at each rate. As a control, the B+N codoped sample with a reverse addition sequence exhibits the lowest discharge capacity. This is even worse than the original LFP/C material.

DOI: 10.1021/acsami.5b05398
ACS Appl. Mater. Interfaces 2015, 7, 20134−20143

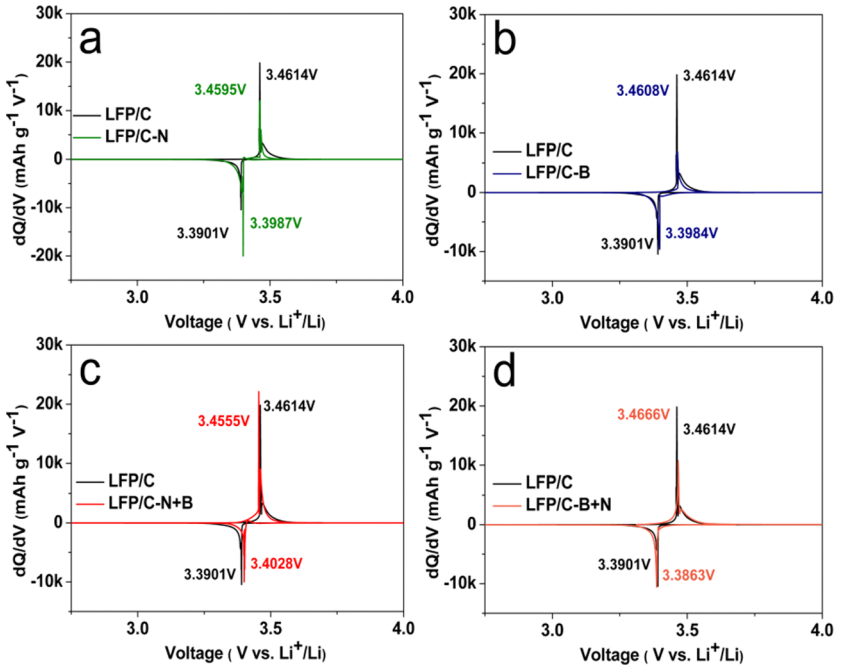

Figure 7. Differential capacity (dQ/dV) as a function of potential (V) for the samples LFP/C, LFP/C−N, LFP/C−B, LFP/C−N+B, and LFP/C−B+N at 0.1C.

The cycling performance of various samples at 20 C is shown in Figure 6. In the initial cycle, the discharge capacity of LFP/C, LFP/C−N, LFP/C−B, LFP/C−N+B, and LFP/C−B+N is 101.1, 104.7, 104.8, 121.6, and 95.4 mAh g^{-1}, respectively. This decreases to 77.4, 81.7, 82.2, 96.9, and 73.7 mAh g^{-1} after 50 cycles of charging/discharging, keeping 76.4%, 78.0%, 78.4%, 79.6%, and 77.2% retention, respectively, relative to the initial cycle. The N+B codoped sample exhibits superior electrochemical performance.

To shed light on the polarization effect of various samples, i.e., the voltage gap between the charge and discharge plateaus, we employed differential capacity versus potential ($dQ/dV \sim V$) of the five samples. As demonstrated in Figure 7a−d, the different polarization peaks of each sample are quite obvious in the voltage area of 2.0−4.2 V at the rate of 0.1 C (to make the boundary clear, the *X*-axis has been stretched to 2.75−4.0 V). The two polarization peaks concerning oxidation and reduction potentials are clearly shown to reveal the voltage value of $LiFePO_4/FePO_4$ phase transition.[41,42] The as-prepared LFP/C displays the dQ/dV potential of oxidation plateau peak at 3.4614 V ($LiFePO_4$ converting to $FePO_4$ during charging), and the reduction peak at 3.3901 V ($FePO_4$ back to $LiFePO_4$ during discharging). In comparison, the charging/discharging peaks of LFP/C−N, LFP/C−B, LFP/C−N+B, and LFP/C−B+N are surrounded at 3.4595/3.3987 V, 3.4608/3.3984 V, 3.4555/3.4028 V, and 3.4666/3.3863 V, respectively. The lower the potential gap, the better the reversibility seen in the reaction. It is clear that the voltage gap between charging and discharging potentials (i.e., the polarization) is much larger for LFP/C−B+N (80.3 mV) vs LFP/C (71.3 mV), LFP/C−B (62.4 mV), LFP/C−N (60.8 mV), and LFP/C−N+B (52.7 mV), indicating that the kinetics of $LiFePO_4$ is enhanced with positive doping.

The electrochemical properties of single-doped and codoped samples based on commercial c-LFP/C are shown in Figure S10. At the rate of 0.1 C, the initial discharge capacity of c-LFP/C, c-LFP/C−N, and c-LFP/C−B is 141.4, 147.9, and 146.5 mAh g^{-1}, respectively, and the codoped sample c-LFP/C−N+B elevates it up to 165.7 mAh g^{-1} (Figure S10a). With increase of current rates (Figure S10b), c-LFP/C−N+B displays better performance versus single doping, which coincide with the electrochemical performance above. This indicates that there exists small polarization in the electrode for single-doped and codoped samples, and the enhancement effect becomes evident as the charge/discharge rate increases. Figure S11 shows the cycling performance at 20 C: the N+B codoped sample keeps the retention rate of nearly 100% (78.4 to 78.4 mAh g^{-1}) compared with the c-LFP/C of 78.6% (48.1 to 37.8 mAh g^{-1}), c-LFP/C−N of 92.5% (64.2 to 59.4 mAh g^{-1}), c-LFP/C−B of 85.5% (58.5 to 50 mAh g^{-1}), and c-LFP/C−B+N 88.4% (40.6 to 35.9 mAh g^{-1}) after 500 cycles. Therefore, the synergistic effect of nitrogen and boron in carbon can efficiently enhance the electrochemical performance of commercial $LiFePO_4$ likewise.

The above results concerning capacity indicate that the successful single N- or B-doping or the N+B codoping into the carbon layer of the material can not only elevate the capacity at high current rates and strengthen the performance of the materials, but also create synergistic effect of nitrogen and boron (in the absence of N−B impurities).

Incorporated with the above electronic performance analysis, it is reasonable to conclude that the improved electrochemical performance of single N-doped LFP/C materials is attributed to the good electron donors of nitrogen additives that can provide adequate free carriers to increase the conductivity of the sample coated with carbon. For single B-doped LFP/C materials, the improved electrochemical property is due to the good electron acceptors (hole-type charge carriers) generated by boron additives.[23] The literature indicates that codoping nitrogen and boron into carbon layers can create synergistic effect because of unique electronic structure,[33] owing to the electronegativity order of N (3.04) > C (2.55) > B (2.04) besides their analogous atomic sizes with respect to carbon. In the case of N+B codoped LFP/C materials, the excellent electrochemical performance is attributed to the synergistic

DOI: 10.1021/acsami.5b05398
ACS Appl. Mater. Interfaces 2015, 7, 20134−20143

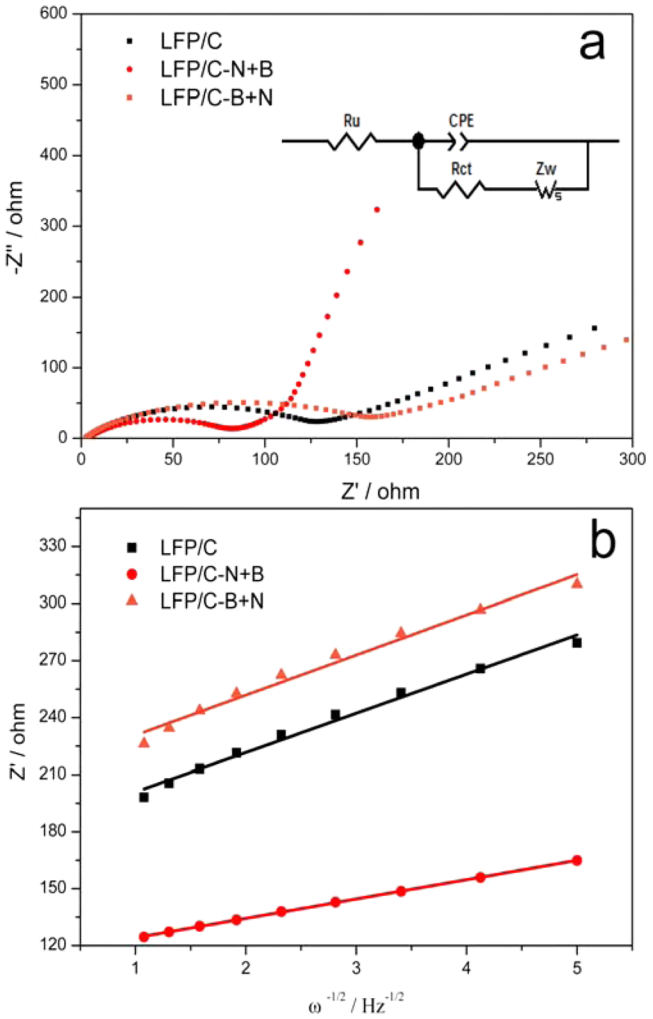

Figure 8. (a) Equivalent circuit and EIS of LFP/C, LFP/C−N+B, and LFP/C−B+N; (b) the relationship between Z' and reciprocal square root of frequency ($\omega^{-1/2}$).

effect of nitrogen and boron additives. With the coexistence of electron donors and electron acceptors, it is much easier for electrons to migrate from the $LiFePO_4$ surface to the carbon layer during charging, and then move back from carbon coatings to the $LiFePO_4$ surface during discharging.

To deeply understand the remarkably high rate of performance of boron and nitrogen codoped materials (LFP/C−N+B and c-LFP/C−N+B) and their counterparts (LFP/C−B+N and c-LFP/C−B+N) compared with the original materials (LFP/C and c-LFP/C) without the doping method, we measured electrochemical impedance spectroscopy (EIS). First, the EIS data is simulated through the equivalent circuit in Figure 8a, in which R_u represents the uncompensated resistance that includes contributions of electrolyte, particle−particle contact, and the resistance between the electrode and the current collector. R_{ct} refers to charge transfer resistance that is related to the electrochemical reaction at the electrode−electrolyte interface and particle−particle contact.[43,44] The CPE (constant phase angle element) represents the constant phase element concerning dispersion effect caused by the heterogeneous structure. Figure 8a and Figure S12a illustrate the EIS spectra, which consist of a semicircle at the high frequency region attributed to the electrochemical charge-transfer reaction, and an oblique straight line at the low frequency corresponding to the diffusion of lithium ions into the bulk of the anode material (Warburg diffusion Z_w). Through the Nyquist plot, we can easily notice that the semicircle diameters of the original materials are shorter than that of the B+N codoped samples and longer than the N+B codoped materials. After fitting by Zview software with an equivalent circuit using impedance spectra, we find that the charge transfer resistance values (R_{ct}) of the B+N codoped samples are the highest in both of the materials due to the nonconducting impurities (N−B configuration). This decreases from 126.5Ω in LFP/C to 84.3Ω in LFP/C−N+B, and 260.4Ω in c-LFP/C to 216.3Ω in c-LFP/C−N+B, indicating that the electron-type charge carrier donated by nitrogen atoms, together with the hole-type carrier attributed by boron atoms, can reduce the charge transfer impedance and conquer the dynamic limitations of electrode process. Ultimately, this improves the electrochemical performance in the modified electrode. The results including R_u, CPE, R_{ct} and Z_w are shown in Table 5.

The exchange current density ($i_0 = RT/nFR_{ct}$) is used to measure the activity of the electrodes. Generally, the electrochemical reaction with higher i_0 value tends proceeded much more easily and is more difficult with polarization. The i_0 values of LFP/C−N+B (0.30 mA) and c-LFP/C−N+B (0.12 mA) are higher than those of LFP/C (0.20 mA) and c-LFP/C (0.10 mA), and also LFP/C−B+N (0.16 mA) and c-LFP/C−B+N (0.09 mA). This coincides with the outstanding electrochemical performance. The diffusion coefficients (D) of Li^+ are calculated with the equation

$$D = \frac{R^2T^2}{2A^2n^4F^4C^2\sigma^2} \quad (1)$$

where R refers to the gas constant, T is the absolute temperature, A is the surface area of the cathode, n is the number of electrons per molecule during oxidization, F is the Faraday constant, C is the concentration of lithium ion, and σ is the Warburg factor which is relative to Z'

$$Z' = R_D + R_L + \sigma\omega^{-1/2} \quad (2)$$

where R_D refers to the resistance of charge transfer, and R_L is the solution resistance.

The relationship between Z' and $\omega^{-(1/2)}$ in the low frequency is shown in Figure 8b and Figure S12b, and the results of the lithium ion diffusion coefficients are 9.46×10^{-14}, 3.86×10^{-13}, and 9.03×10^{-14} $cm^2\ s^{-1}$ for LFP/C, LFP/C−N+B, and LFP/C−B+N; and 1.28×10^{-13}, 2.05×10^{-13}, and 2.8×10^{-14} $cm^2\ s^{-1}$ for c-LFP/C, c-LFP/C−N+B, and c-LFP/C−B+N, respectively. This suggests that the lithium ions float more in codoped sample, which is responsible for its better electrochemical performance. As discussed above, the EIS results further confirm that the

Table 5. Fitting Results Using Sectionalized Simulation

sample	R_u	CPE-T/ $\times 10^{-5}$	CPE-P	R_{ct}	Z_w-R	Z_w-T	Z_w-P	error/%
LFP/C	2.639	4.763	0.7477	126.5	660.9	30.99	0.507	1.00
LFP/C−N+B	2.451	5.165	0.7181	84.3	907.3	4.725	0.7403	0.92
LFP/C−B+N	2.895	6.340	0.6976	160.5	505.5	25.66	0.5017	0.99

DOI: 10.1021/acsami.5b05398
ACS Appl. Mater. Interfaces 2015, 7, 20134−20143

carbon layers with nitrogen and boron codoping can improve the electrochemical conductivity of $LiFePO_4$.

4. CONCLUSIONS

We have successfully synthesized the single N- or B-doped and the boron and nitrogen codoped $LiFePO_4$/C materials using a simple ball-milling process followed by calcination. These were then successfully applied to the existing commercial $LiFePO_4$, both of which offer excellent high rates of electrochemical performance. The electronic conductivity and the electrochemical performance can be improved through single nitrogen doping or boron doping. The boron and nitrogen codoped $LiFePO_4$/C materials show that the electrochemical performance is susceptible to the addition sequence. The N+B type codoped carbon coating on the material can generate the synergistic effect to elevate the high-rate capacity much higher than the sum of single doping. This is attributed to the electron-type and the hole-type carrier donated by nitrogen and boron atoms. At a high rate of 20 C, the LFP/C−N+B sample can improve the discharge capacity from 101.1 mAh g^{-1} to 121.6 mAh g^{-1}, and the c-LFP/C−N+B can elevate the discharge capacity to 78.4 mAh g^{-1} rather than 48.1 mAh g^{-1}. This markedly enhances the electrochemical performance of both commercial and experimental products. The $LiFePO_4$ with N+B type codoped carbon coating exhibits a significant enhancement at high current rates and in retention rates. This is promising for commercial lithium ion batteries.

■ ASSOCIATED CONTENT

Supporting Information

The Supporting Information is available free of charge on the ACS Publications website at DOI: 10.1021/acsami.5b05398.

Varieties of molar ratio toward nitrogen (and boron) to carbon, the charge−discharge profiles at 0.1 C and the multirate capacity of doping (codoping) products based on LFP/C and c-LFP/C, the EIS figure of samples based on c-LFP/C, the powder electronic conductivity and the I_D/I_G value of five samples based on c-LFP/C. (PDF)

■ AUTHOR INFORMATION

Corresponding Author

*E-mail: liwei@tju.edu.cn. Tel: +86-22-27890643. Fax: +86-22-27890643.

Notes

The authors declare no competing financial interest.

■ ACKNOWLEDGMENTS

The work is financially supported by the Special Funds for Major State Basic Research Program of China (2012CB720300), NSFC (21476158), and Program for Changjiang Scholars and Innovative Research Team in University (IRT1161).

■ REFERENCES

(1) Tarascon, J. M.; Armand, M. Issues and Challenges Facing Rechargeable Lithium Batteries. *Nature* **2001**, *414*, 359−367.

(2) Nishimura, S.; Kobayashi, G.; Ohoyama, K.; Kanno, R.; Yashima, M.; Yamada, A. Experimental Visualization of Lithium Diffusion in Li_xFePO_4. *Nat. Mater.* **2008**, *7*, 707−711.

(3) Chen, J. M.; Hsu, C. H.; Lin, Y. R.; Hsiao, M. H.; Fey, G. T. K. High-Power $LiFePO_4$ Cathode Materials with a Continuous Nano Carbon Network for Lithium-ion Batteries. *J. Power Sources* **2008**, *184*, 498−502.

(4) Jinli, Z.; Jiao, W.; Yuanyuan, L.; Ning, N.; Junjie, G.; Feng, Y.; Wei, L. High-Performance Lithium iron Phosphate with Phosphorus-Doped Carbon Layers for Lithium Ion Batteries. *J. Mater. Chem. A* **2015**, *3*, 2043−2049.

(5) Yu, F.; Zhang, L. L.; Li, Y. C.; An, Y. X.; Zhu, M. Y.; Dai, B. Mechanism Studies of $LiFePO_4$ Cathode Material: Lithiation/Delithiation Process, Electrochemical Modification and Synthetic Reaction. *RSC Adv.* **2014**, *4*, 54576−54602.

(6) Zou, H. L.; Zhang, G. H.; Shen, P. K. Intermittent Microwave Heating Synthesized High Performance Spherical $LiFePO_4$/C for Li-ion Batteries. *Mater. Res. Bull.* **2010**, *45*, 149−152.

(7) Wang, L.; Huang, Y. D.; Jiang, R. R.; Jia, D. Z. Nano-$LiFePO_4$/MWCNT Cathode Materials Prepared by Room-Temperature Solid-State Reaction and Microwave Heating. *J. Electrochem. Soc.* **2007**, *154*, A1015−A1019.

(8) Liu, S. Q.; Gong, B. L.; Huang, K. L.; Zhang, G.; Li, S. C. Synthesis of $LiFePO_4$/C Composite Cathode Materials by a Novel Carbothermal Reduction Method and its Performance. *J. Inorg. Mater.* **2007**, *22*, 283−286.

(9) Fan, C. L.; Han, S. C.; Li, L. F.; Bai, Y. M.; Zhang, K. H.; Chen, J.; Zhang, X. Structure and Electrochemical Performances of $LiFe_{1-2x}Ti_xPO_4$/C Cathode Doped with High Valence Ti^{4+} by Carbothermal Reduction Method. *J. Alloys Compd.* **2013**, *576*, 18−23.

(10) Pang, L. J.; Zhao, M. S.; Zhao, X.; Chai, Y. J. Preparation and Electrochemical Performance of Gd-Doped $LiFePO_4$/C Composites. *J. Power Sources* **2012**, *201*, 253−258.

(11) Deng, C.; Zhang, S.; Yang, S. Y.; Fu, B. L.; Ma, L. Synthesis and Characterization of $Li_2Fe_{0.97}M_{0.03}SiO_4$ (M = Zn^{2+}, Cu^{2+}, Ni^{2+}) Cathode Materials for Lithium ion Batteries. *J. Power Sources* **2011**, *196*, 386−392.

(12) Murugan, A. V.; Muraliganth, T.; Manthiram, A. One-Pot Microwave-Hydrothermal Synthesis and Characterization of Carbon-Coated $LiMPO_4$ (M = Mn, Fe, and Co) Cathodes. *J. Electrochem. Soc.* **2009**, *156*, A79−A83.

(13) Dominko, R.; Gaberscek, M.; Drofenik, J.; Bele, M.; Pejovnik, S.; Jamnik, J. The role of Carbon Black Distribution in Cathodes for Li ion Batteries. *J. Power Sources* **2003**, *119*, 770−773.

(14) Ravet, N.; Chouinard, Y.; Magnan, J. F.; Besner, S.; Gauthier, M.; Armand, M. Electroactivity of Natural and Synthetic Triphylite. *J. Power Sources* **2001**, *97−8*, 503−507.

(15) Shi, Y.; Chou, S. L.; Wang, J. Z.; Wexler, D.; Li, H. J.; Liu, H. K.; Wu, Y. P. Graphene Wrapped $LiFePO_4$/C Composites as Cathode Materials for Li-ion Batteries with Enhanced Rate Capability. *J. Mater. Chem.* **2012**, *22*, 16465−16470.

(16) Wu, Y. P.; Rahm, E.; Holze, R. Effects of Heteroatoms on Electrochemical Performance of Electrode Materials for Lithium ion Batteries. *Electrochim. Acta* **2002**, *47*, 3491−3507.

(17) Chen, S.; Duan, J. J.; Jaroniec, M.; Qiao, S. Z. Nitrogen and Oxygen Dual-Doped Carbon Hydrogel Film as a Substrate-Free Electrode for Highly Efficient Oxygen Evolution Reaction. *Adv. Mater.* **2014**, *26*, 2925−2930.

(18) Duan, J. J.; Zheng, Y.; Chen, S.; Tang, Y. H.; Jaroniec, M.; Qiao, S. Z. Mesoporous Hybrid Material Composed of Mn_3O_4 Nanoparticles on Nitrogen-Doped Graphene for Highly Efficient Oxygen Reduction Reaction. *Chem. Commun.* **2013**, *49*, 7705−7707.

(19) Qie, L.; Chen, W. M.; Wang, Z. H.; Shao, Q. G.; Li, X.; Yuan, L. X.; Hu, X. L.; Zhang, W. X.; Huang, Y. H. Nitrogen-Doped Porous Carbon Nanofiber Webs as Anodes for Lithium ion Batteries with a Superhigh Capacity and Rate Capability. *Adv. Mater.* **2012**, *24*, 2047−2050.

(20) Yoon, S.; Liao, C.; Sun, X. G.; Bridges, C. A.; Unocic, R. R.; Nanda, J.; Dai, S.; Paranthaman, M. P. Conductive Surface Modification of $LiFePO_4$ with Nitrogen-Doped Carbon Layers for Lithium-ion Batteries. *J. Mater. Chem.* **2012**, *22*, 4611−4614.

(21) Yang, J. L.; Wang, J. J.; Li, X. F.; Wang, D. N.; Liu, J.; Liang, G. X.; Gauthier, M.; Li, Y. L.; Geng, D. S.; Li, R. Y.; Sun, X. L. Hierarchically Porous $LiFePO_4$/Nitrogen-Doped Carbon Nanotubes Composite as a Cathode for Lithium ion Batteries. *J. Mater. Chem.* **2012**, *22*, 7537−7543.

DOI: 10.1021/acsami.5b05398
ACS Appl. Mater. Interfaces 2015, 7, 20134−20143

(22) Liu, H.; Zhang, Y.; Li, R. Y.; Sun, X. L.; Desilets, S.; Abou-Rachid, H.; Jaidann, M.; Lussier, L. S. Structural and Morphological Control of Aligned Nitrogen-Doped Carbon Nanotubes. *Carbon* **2010**, *48*, 1498−1507.
(23) Wang, C.; Guo, Z. Y.; Shen, W.; Xu, Q. J.; Liu, H. M.; Wang, Y. G. B-doped Carbon Coating Improves the Electrochemical Performance of Electrode Materials for Li-ion Batteries. *Adv. Funct. Mater.* **2014**, *24*, 5511−5521.
(24) Liu, Y. Y.; Gu, J. J.; Zhang, J. L.; Wang, J.; Nie, N.; Fu, Y.; Li, W.; Yu, F. Controllable Synthesis of Nano-sized $LiFePO_4$/C via a High Shear Mixer Facilitated Hydrothermal Method for High Rate Li-ion Batteries. *Electrochim. Acta* **2015**, *173*, 448−457.
(25) Raymundo-Pinero, E.; Cazorla-Amoros, D.; Linares-Solano, A.; Find, J.; Wild, U.; Schlogl, R. Structural Characterization of N-Containing Activated Carbon Fibers Prepared from a Low Softening Point Petroleum pitch and a Melamine Resin. *Carbon* **2002**, *40*, 597−608.
(26) Zheng, Y.; Jiao, Y.; Ge, L.; Jaroniec, M.; Qiao, S. Z. Two-Step Boron and Nitrogen Doping in Graphene for Enhanced Synergistic Catalysis. *Angew. Chem., Int. Ed.* **2013**, *52*, 3110−3116.
(27) Franke, R.; Chassé, Th.; Streubel, P.; Meisel, A. Auger Parameters and Relaxation Energies of Phosphorus in Solid Compounds. *J. Electron Spectrosc. Relat. Phenom.* **1991**, *56*, 381−388.
(28) Jo, G.; Shanmugam, S. Single-Step Synthetic Approach for Boron-Doped Carbons as a Non-Precious Catalyst for Oxygen Reduction in Alkaline Medium. *Electrochem. Commun.* **2012**, *25*, 101−104.
(29) Zhao, Y.; Yang, L. J.; Chen, S.; Wang, X. Z.; Ma, Y. W.; Wu, Q.; Jiang, Y. F.; Qian, W. J.; Hu, Z. Can Boron and Nitrogen Co-Doping Improve Oxygen Reduction Reaction Activity of Carbon Nanotubes? *J. Am. Chem. Soc.* **2013**, *135*, 1201−1204.
(30) Ozaki, J.; Kimura, N.; Anahara, T.; Oya, A. Preparation and Oxygen Reduction Activity of BN-Doped Carbons. *Carbon* **2007**, *45*, 1847−1853.
(31) Kwon, T.; Nishihara, H.; Itoi, H.; Yang, Q. H.; Kyotani, T. Enhancement Mechanism of Electrochemical Capacitance in Nitrogen-/Boron-Doped Carbons with Uniform Straight Nanochannels. *Langmuir* **2009**, *25*, 11961−11968.
(32) Wang, S. Y.; Zhang, L. P.; Xia, Z. H.; Roy, A.; Chang, D. W.; Baek, J. B.; Dai, L. M. BCN Graphene as Efficient Metal-Free Electrocatalyst for the Oxygen Reduction Reaction. *Angew. Chem., Int. Ed.* **2012**, *51*, 4209−4212.
(33) Wu, T. R.; Shen, H. L.; Sun, L.; Cheng, B.; Liu, B.; Shen, J. C. Nitrogen and Boron Doped Monolayer Graphene by Chemical Vapor Deposition using Polystyrene, Urea and Boric Acid. *New J. Chem.* **2012**, *36*, 1385−1391.
(34) Zheng, B.; Hermet, P.; Henrard, L. Scanning Tunneling Microscopy Simulations of Nitrogen- and Boron-Doped Graphene and Single-Walled Carbon Nanotubes. *ACS Nano* **2010**, *4*, 4165−4173.
(35) Sun, C.; Yan, L. M.; Yue, B. H. Improvement of Surface Structure and Enhancement of Conductivity of $LiFePO_4$ Surface by Graphene and Graphene-Like B-C-N Coating. *Acta Phys.-Chim. Sin.* **2013**, *29*, 1666−1672.
(36) Fisher, C. A. J.; Islam, M. S. Surface Structures and Crystal Morphologies of $LiFePO_4$: Relevance to Electrochemical Behaviour. *J. Mater. Chem.* **2008**, *18*, 1209−1215.
(37) Wu, Z. S.; Ren, W. C.; Gao, L. B.; Zhao, J. P.; Chen, Z. P.; Liu, B. L.; Tang, D. M.; Yu, B.; Jiang, C. B.; Cheng, H. M. Synthesis of Graphene Sheets with High Electrical Conductivity and Good Thermal Stability by Hydrogen Arc Discharge Exfoliation. *ACS Nano* **2009**, *3*, 411−417.
(38) Guo, B. D.; Liu, Q. A.; Chen, E. D.; Zhu, H. W.; Fang, L. A.; Gong, J. R. Controllable N-Doping of Graphene. *Nano Lett.* **2010**, *10*, 4975−4980.
(39) Mukhopadhyay, I.; Hoshino, N.; Kawasaki, S.; Okino, F.; Hsu, W. K.; Touhara, H. Electrochemical Li Insertion in B-Doped Multiwall Carbon Nanotubes. *J. Electrochem. Soc.* **2002**, *149*, A39−A44.
(40) Wu, Z. S.; Winter, A.; Chen, L.; Sun, Y.; Turchanin, A.; Feng, X. L.; Mullen, K. Three-Dimensional Nitrogen and Boron Co-Doped Graphene for High-Performance All-Solid-State Supercapacitors. *Adv. Mater.* **2012**, *24*, 5130−5135.
(41) Yu, F.; Zhang, L. L.; Lai, L. F.; Zhu, M. Y.; Guo, Y. C.; Xia, L. L.; Qi, P. R.; Wang, G.; Dai, B. High Electrochemical Performance of $LiFePO_4$ Cathode Material via In-Situ Microwave Exfoliated Graphene Oxide. *Electrochim. Acta* **2015**, *151*, 240−248.
(42) Yu, F.; Lim, S. H.; Zhen, Y. D.; An, Y. X.; Lin, J. Y. Optimized Electrochemical Performance of Three-Dimensional Porous $LiFePO_4$/C Microspheres via Microwave Irradiation Assisted Synthesis. *J. Power Sources* **2014**, *271*, 223−230.
(43) Shin, H. C.; Cho, W. I.; Jang, H. Electrochemical Properties of Carbon-Coated $LiFePO_4$ Cathode using Graphite, Carbon Black, and Acetylene Black. *Electrochim. Acta* **2006**, *52*, 1472−1476.
(44) Lee, C. Y.; Tsai, H. M.; Chuang, H. J.; Li, S. Y.; Lin, P.; Tseng, T. Y. Characteristics and Electrochemical Performance of Supercapacitors with Manganese Oxide-Carbon Nanotube Nanocomposite Electrodes. *J. Electrochem. Soc.* **2005**, *152*, A716−A720.

DOI: 10.1021/acsami.5b05398
ACS Appl. Mater. Interfaces 2015, 7, 20134−20143